Kinetics of sickle cell biorheology and implications for painful vasoocclusive crisis

E Du[a,1], Monica Diez-Silva[a], Gregory J. Kato[b], Ming Dao[a,2], and Subra Suresh[c,d,2]

[a]Department of Materials Science and Engineering, Massachusetts Institute of Technology, Cambridge, MA 02139; [b]Department of Medicine, Division of Hematology-Oncology, University of Pittsburgh, Pittsburgh, PA 15261; and Departments of [c]Biomedical Engineering and [d]Materials Science and Engineering, Carnegie Mellon University, Pittsburgh, PA 15213

Contributed by Subra Suresh, December 17, 2014 (sent for review October 27, 2014)

We developed a microfluidics-based model to quantify cell-level processes modulating the pathophysiology of sickle cell disease (SCD). This in vitro model enabled quantitative investigations of the kinetics of cell sickling, unsickling, and cell rheology. We created short-term and long-term hypoxic conditions to simulate normal and retarded transit scenarios in microvasculature. Using blood samples from 25 SCD patients with sickle hemoglobin (HbS) levels varying from 64 to 90.1%, we investigated how cell biophysical alterations during blood flow correlated with hematological parameters, HbS level, and hydroxyurea (HU) therapy. From these measurements, we identified two severe cases of SCD that were also independently validated as severe from a genotype-based disease severity classification. These results point to the potential of this method as a diagnostic indicator of disease severity. In addition, we investigated the role of cell density in the kinetics of cell sickling. We observed an effect of HU therapy mainly in relatively dense cell populations, and that the sickled fraction increased with cell density. These results lend support to the possibility that the microfluidic platform developed here offers a unique and quantitative approach to assess the kinetic, rheological, and hematological factors involved in vasoocclusive events associated with SCD and to develop alternative diagnostic tools for disease severity to supplement other methods. Such insights may also lead to a better understanding of the pathogenic basis and mechanism of drug response in SCD.

sickle cell anemia | vasoocclusion | capillary obstruction ratio | cell deformability | Aes-103

Sickle cell disease (SCD) is characterized by acute and chronic vasoocclusion that can cause pain (1), acute chest syndrome (2), organ damage (3), stroke, and even death (4, 5). The pathogenic basis of "painful crisis" arising from vasoocclusion in SCD is extremely complex (6–8). It is triggered by many factors, including poor deformability of red blood cells (RBCs), adhesion among multiple cell types and blood components (e.g., sickle RBCs, endothelial cells, adherent leukocytes, and possibly platelets), as well as the local microenvironment (e.g., low oxygen concentration and acidosis). Under conditions of low oxygen partial pressure (pO_2), sickle RBCs experience intracellular sickle hemoglobin (HbS) polymerization, thereby reducing cell deformability (9). Such reductions in deformability can severely impact blood flow in narrow vessels, ultimately causing a transient or persistent blockage (10). Competition between the delay time for HbS polymerization and the RBC transit time in microcirculation is likely a key determinant of disease severity (11). Both in vitro (12) and ex vivo (13) models reveal that HbS polymerization and its effect on cellular rigidity play important roles in causing vascular obstruction. For example, HbS polymerization alone could be sufficient to cause complete RBC blockage in vasculature (12). Increases in microvascular transit time, arising from higher rigidity, of sickle RBCs cause peripheral vascular resistance to blood flow (13).

The search for better means to predict painful vasoocclusion crises has focused on a range of hematological and rheological abnormalities. Significant correlations have been shown between pain rates and early death in patients with sickle cell anemia (14) and between early death and several risk factors such as fetal hemoglobin (HbF), hematocrit, and white cell count (15). However, factors such as patient age, sex, HbF (16), intracellular HbS polymerization (17), or fraction of dense RBCs (18) do not appear to show a sufficiently direct correlation with the frequency and/or severity of pain crises. Although HbF level is generally considered important, its direct connection to disease severity is not fully established (19, 20). Some possible links between the incidence of painful crises and steady-state cell hydration (21) and/or deformability at isotonic osmolarity have been identified (22). Such connections, however, do not account for the observation that cell deformability and the proportion of dense cells vary longitudinally in the same patient during crisis (23). Changes have also been reported in the biorheological characteristics of sickle RBC suspension following deoxygenation (DeOxy) in an in vitro vascular model (24).

An in vitro model with a well-defined vascular structure and a well-controlled hypoxia condition would serve as an ideal tool to investigate many complex pathophysiological processes in vasoocclusion. Recent advances in microfluidics technology have enabled us to design unique in vitro capabilities with biophysically appropriate microenvironments that mimic the geometric features of vascular systems, thereby facilitating quantitative characterization of DeOxy blood flow (12, 24), detection of HbS polymerization in DeOxy liquid drops (25), and investigation of pathologic adhesion in blood rheology (26). Several methods

Significance

A major challenge with in vitro investigations of the pathophysiological processes in sickle cell disease (SCD) has been the lack of a well-controlled microenvironment to mimic in vivo circulating conditions. The microfluidic platform developed here provides a quantitative assay of the kinetics of cell sickling, unsickling, and single-cell rheology. The ensuing alterations in the biorheological characteristics of sickle cells under hypoxic conditions show strong correlation with sickle hemoglobin level, hydroxyurea (HU) therapy, and cell density. These analyses provide cell-level perspectives of the clinical manifestations in SCD patients and offer unique diagnostic indicators of vasoocclusion and disease severity. These results could also provide alternative pathways to supplement current clinical practices to evaluate HU therapy.

Author contributions: E.D., M.D.-S., G.J.K., M.D., and S.S. designed research; E.D. and M.D.-S. performed research; E.D., M.D.-S., G.J.K., M.D., and S.S. analyzed data; and E.D., M.D.-S., G.J.K., M.D., and S.S. wrote the paper.

Conflict of interest statement: E.D., M.D.-S., M.D., and S.S. have filed a patent based on the work presented in this paper.

Freely available online through the PNAS open access option.

[1]Present address: Department of Ocean and Mechanical Engineering, Florida Atlantic University, Boca Raton, FL 33431.

[2]To whom correspondence may be addressed. Email: mingdao@mit.edu or suresh@cmu.edu.

This article contains supporting information online at www.pnas.org/lookup/suppl/doi:10.1073/pnas.1424111112/-/DCSupplemental.

www.pnas.org/cgi/doi/10.1073/pnas.1424111112

have been developed to mimic oxygen depletion whereby HbS polymerization and subsequent cell sickling can be triggered; they include long-term gas perfusion at low pO_2 level (13, 27), DeOxy medium exchange (25, 28), reducing agents (29–31), and laser photodissociation of carbon monoxide (22, 32). Along with complex in vivo models that reflect the dynamic response of cells, an in vitro model would have the potential to predict the conditions that would lead to vasoocclusion and to improve the assessment of disease severity by quantifying the individual parameters that modulate vasoocclusion.

We designed a microfluidic platform (Fig. 1) that mimics the rheology of microcirculation in vivo. It also characterizes the isolated effects of cell morphologic sickling, unsickling, and altered cell rheology. With this design, we explored in a systematic and controlled manner possible correlations of these effects with hematological parameters (e.g., %HbS), cell density, and hydroxyurea (HU) therapy.

Cell sickling was measured using a double-layer device with a cell channel (5 μm high), a gas channel (100 μm high), and an in-between polydimethylsiloxane (PDMS) film 150 μm in thickness (Fig. 1*A*). The O_2 concentration was controlled by exchanging gas flow in the channel through the PDMS membrane, which is gas-permeable (33). Although it is known (34) that the morphology of sickled cells depends on the DeOxy rate, we observed heterogeneity in cell morphology at the same DeOxy rate. Sickle RBCs typically form spiky edges and dark coarse texture due to intracellular HbS polymerization, the visual identification of which was enhanced by a band-pass filter (Fig. 1*B* and Movie S1). We thus define sickled cells as those obviously distorted from their original shape and/or texture under the Oxy state [O_2 concentration ~20% (vol/vol)] to the DeOxy state (O_2 concentration <5%). This visual determination of cell sickling was further confirmed with an independent single-cell rheology test, where similar trends were observed in cell sickling and single-cell capillary obstruction (*Results*). The kinetics of cell sickling was quantified by two parameters: the sickled fraction (the fraction of all RBCs in the sample that are sickled) and the delay time of cell sickling (the time elapsed between the initiation of DeOxy and the point when a cell shows optically visible features of morphologic sickling). The delay time of cell unsickling was defined as the time elapsed between the initiation of reoxygenation (ReOxy) and the point when the RBC fully recovered its presickle morphology in a visibly identifiable manner.

Individual-cell rheology was measured using a microfluidic channel that consisted of periodic obstacles forming microgates 4 μm wide, 5 μm deep, and 15 μm long (Fig. 1*C*). The channel dimensions were chosen to mimic the size of the smallest capillaries in the human body (4–10 μm in diameter) (35). Cell velocity was measured as the average velocity of individual RBCs flowing through periodic gates under a constant differential pressure. The obstruction fraction was determined as the ratio of obstructed RBCs to all RBCs entering into the microgate arrays during the DeOxy period.

Results

Kinetics of Cell Sickling and Unsickling. Kinetics of individual cell sickling and unsickling under transient hypoxia conditions was quantified by the delay time and maximum sickled fraction on 25 SCD patient samples: 7 patients without HU therapy (off-HU) and 18 patients with HU therapy (on-HU) (*SI Text*, *Patient's HU Status*). Short-term and long-term hypoxia conditions were created to simulate normal and retarded transit scenarios in microvasculature (Fig. 2 *A* and *B*). Representative cell sickling profiles upon changes in O_2 concentration are shown (Fig. 2*C*). Compared with the relatively long sickling process (>100 s for a sickled fraction rising from zero to a saturated, maximum level), the unsickling process after ReOxy was much faster (<20 s for a sickled fraction reducing from the saturated level to zero), disregarding the small discrepancy in the DeOxy and ReOxy rates (<20 s). This observation applied to all patient samples tested.

Results of the kinetics of cell sickling were plotted against the %HbS of individual patients (Fig. 3). The delay time of sickling was greater than 25 s for RBCs (i.e., for reaching 5% sickled fraction) for most of the samples in the study (Fig. 3*A*). The delay time of sickling for the on-HU group was significantly longer than that for the off-HU group ($P < 0.01$). Within the on-HU group, the delay times of sickling (for the 5% sickled fraction) varied from 28 to 100 s, suggesting a difference in the efficacy of HU among different patients. Similar trends were observed at a higher sickled fraction (10%; Fig. 3*B*). Six cases showed significantly longer delay times (>60 s) than the others, suggesting a possible beneficial effect of HU therapy. The two cases with the shortest delay time (less than 25 s) of cell sickling, marked by arrows (Fig. 3*C*), suggest higher risk for vasoocclusion. For the sickled fraction of each sample reaching its saturated level under the long-term DeOxy state, delay time of cell sickling varied widely within the same patient and among different patients. The influence of HU therapy was statistically significant for the sickling process ($P < 0.02$; Fig. S1*A*). The distribution of delay times of cell unsickling seemed to be random among different patients, and no significant difference was found between the on-HU and off-HU groups ($P = 0.24$; Fig. S1*B*).

Under the short-term DeOxy state, the maximum sickled fraction for all on-HU samples was below 15%, which was significantly lower than that for the off-HU group ($P = 0.03$; Fig. 3*C*). Within the off-HU group, the sickled fraction was highly variable among patients, ranging from less than 10% to over 60%. The two outliers with the most severely shortened delay time results showed consistency with the highest sickled fractions (Fig. 3 *A*–*C*). On the other hand, during the long-term DeOxy

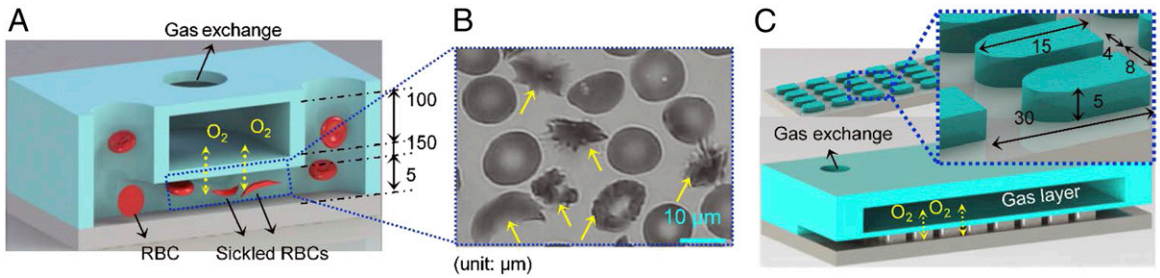

Fig. 1. Microfluidic platform for investigation of biophysical alterations in sickle RBCs under transient hypoxia conditions. (*A*) Schematic of microfluidic device with O_2 control for studying kinetics of cell sickling and unsickling. (*B*) Identification of cell sickling events from a microscopic image (arrows indicate sickled RBCs). (*C*) Schematic of microfluidic device with capillary-inspired structures for single-cell rheology study. Note: Schematics are not drawn to scale, and the dimensions are in microns.

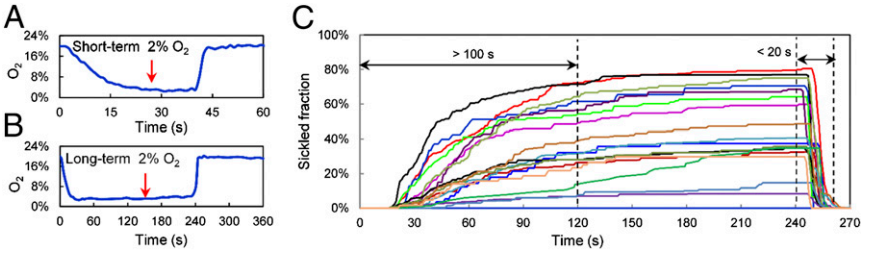

Fig. 2. Profiles of cell sickling and unsickling under transient hypoxia conditions with 2% for the lowest O_2 concentration. (*A* and *B*) Profile of short-term transient DeOxy (O_2 concentration less than 5% for ~25 s) (*A*) and profile of long-term DeOxy (O_2 concentration less than 5% for ~220 s) (*B*). (*C*) Profiles of the sickled fraction of multiple SCD samples during long-term transient DeOxy (each curve represents an individual patient sample).

state, the maximum sickled fraction showed a strong positive correlation with the HbS level (Pearson's correlation coefficient, $R = 0.79$, $P < 0.001$; Fig. 3*D*). The levels of sickled fractions under short-term and long-term DeOxy states are comparable to previous in vitro sickling studies (36, 37) under extended DeOxy time [from 1 to 5 h of incubation under 4% O_2 (36) or 2 h of incubation under 2% O_2 (37)]. The discrepancy in DeOxy time may be due to the rapid O_2 exchange in the cell suspension using our microfluidic system rather than the static DeOxy incubation system in the earlier studies (36, 37). The result of kinetics of cell sickling correlating with HbF level had a relatively weaker trend in the opposite direction from that with HbS level (e.g., $R = –0.55$, $P = 0.004$ for the sickled fraction under the long-term DeOxy state).

Individual Sickle RBC Rheology. Individual sickle RBC rheology was examined, at a given pressure differential and with a short-term transient hypoxia, as a potential diagnostic indicator of risk for vasoocclusion (Movie S2). Sickle RBCs were deformable during the initial 12 s (O_2 concentration >5%). Here deformability denotes the ability of the cell to successfully traverse the 4-μm-wide microgates. When the O_2 concentration was reduced to less than 5%, the RBCs undergoing sickling were unable to traverse the microgates, thereby causing obstruction to RBC flow. With ReOxy, the obstructed RBCs recovered their shape and deformability, and flow was resumed. The velocity of sickle RBCs was then quantified as the average speed over five microgates for the individual RBCs traveling through the periodic microgates. A representative distribution of cell velocities in response to transient hypoxia is shown (Fig. 4*B*). The velocity of individual sickle RBCs varied widely in the same patient and among different patients. Significant correlation was found between cell velocity and the mean corpuscular volume (MCV; Pearson's $R = –0.89$, $P < 0.001$) (*SI Text*, *Single-Cell Rheology* and Fig. S2). The capillary obstruction ratio was defined as the fraction of the total number of cells that were blocked at the microgates during the DeOxy state. The sickle cell capillary obstruction ratio, measured on six on-HU and six off-HU patient samples, increased with HbS concentration (Fig. 4*C*) similar to that seen with the sickled fraction. In general, the on-HU group exhibited a significantly lower capillary obstruction ratio than the off-HU group ($P = 0.03$). A severe case was identified with the highest capillary obstruction ratio and is marked by an arrow in Fig. 4*C*.

The Role of Cell Density. Previous studies have demonstrated that sickle RBCs have a broad range of cell density from 1.085 to 1.146 g/mL (38–40). To quantify the effects of cell density on the kinetics of cell sickling and unsickling, we categorized sickle RBCs into four populations with average cell densities of 1.086 ± 0.005 g/mL (density 1), 1.095 ± 0.005 g/mL (density 2), 1.105 ± 0.005 g/mL (density 3), and >1.111 g/mL (density 4) for 20 SCD samples from 6 off-HU patients and 14 on-HU patients. The majority of sickle RBCs fell within density 2 and density 3 (Fig. S3*A*). We noticed a significant difference in the sickling growth curve among different density populations of individual blood samples under both short-term and long-term DeOxy states (Fig. S3 *B* and *C*). Results of delay time of cell sickling and sickled fraction were examined along with cell density and the patient's HU status. Delay time of cell sickling decreased with cell density (Fig. 5*A*), which can be rationalized by the hydration state of the cells (41, 42). The mean delay time of cell sickling for the on-HU cases was statistically higher than for off-HU cases ($P < 0.02$). A marked extension in the delay time of cell sickling was seen for densities 3 and 4 with HU therapy ($P = 0.01$ and $P = 0.06$, respectively). The overall delay time for unsickling did not vary significantly among densities 1–3 or between on-HU and off-HU groups (Fig. S4*A*).

The maximum sickled fraction showed a strong correlation with cell density disregarding the patient's HU status or hypoxia duration (Fig. 5*B* and Fig. S4*B*). This observation is consistent with reported correlation between HbS concentration and polymerization kinetics (43, 44). Under short-term hypoxia, HU therapy significantly suppressed sickled fraction, particularly in densities 3 and 4 ($P = 0.01$ and $P = 0.001$, respectively). The

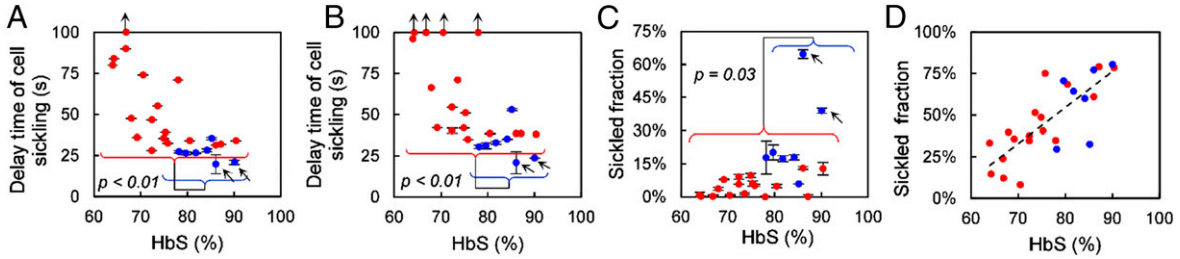

Fig. 3. Kinetics of cell sickling. Delay time of cell sickling (*A*) for 5% sickled fraction and (*B*) for 10% sickled fraction. Distributions of maximum sickled fractions under (*C*) short-term transient DeOxy state (O_2 concentration less than 5% for ~25 s) and (*D*) long-term transient DeOxy state (O_2 concentration less than 5% for ~220 s). Arrows indicate severe cases, defined as those where sickling delay time was less than 25 s. Red circles represent on-HU and blue circles represent off-HU. Error bars indicate standard deviations.

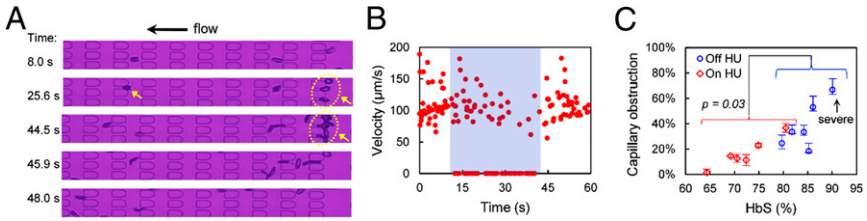

Fig. 4. Individual sickle RBC rheology under transient hypoxia. (*A*) Time sequence of RBCs traveling through capillary-inspired structures. Arrows indicate sickled cells that are unable to pass through the microgates, thereby obstructing RBC flow. (*B*) Representative velocity profile of RBC flow, with each data point representing the average speed of an individual RBC traveling through five of the periodic microgates under a pressure difference of 15 mL water in a 60-mL Terumo plastic syringe tube (equivalent to 22.6 mm H_2O). The shaded area indicates an O_2 concentration lower than 5%. (*C*) Cell capillary obstruction ratio as a function of %HbS. The arrow indicates a severe case with the highest capillary obstruction ratio. Error bars indicate standard deviations.

effects of HbF fractions on density dependence of the cell sickling kinetics show that the differences between the low HbF group (%HbF <15%, $n = 10$) and high HbF group (%HbF >15%, $n = 10$) were not as significant as those between the on-HU and off-HU groups (Fig. S5).

The distribution of Hb types in the density-separated populations was obtained through high performance liquid chromatography (HPLC). The results of 13 patient samples (5 off-HU and 8 on-HU) with HbS levels ranging from 66.8 to 90.4% revealed higher levels of HbS and lower levels of HbF in density 4 than other lighter-density populations (Fig. S6). This observation is consistent with reports that dense cells have higher HbS levels and lower HbF levels than lighter cells (45), and that dense cells have lower HbF levels than all RBCs (46). Surprisingly, there was no significant difference among the three lighter populations for all four Hb types, namely HbS, HbF, HbA (adult Hb), and HbA2 (normal variant of HbA) (Fig. S6*A*). The trends for Hb type vs. cell density were quite similar in both off-HU and on-HU groups (Fig. S6 *B* and *C*). This information seems to contradict the strong correlation of cell sickling with cell density, as it has already been demonstrated that cell sickling is highly dependent on %HbS. To better elucidate this result, we established two parameters to take into account both hydration state and Hb content, including mean intracellular HbS concentration (MCHC-S) and mean intracellular HbF concentration (MCHC-F) (*SI Text*, *MCHC Estimation*). The distribution of MCHC-S increased with cell density (Fig. S6*D*). Density 4 had a high MCHC-S value due to the joint effects of high %HbS and the high MCHC value.

Discussion

Shape change was found to be a reliable marker for cell sickling in hypoxia-induced sickled human RBCs at 37 °C (36, 37), although an earlier study argued otherwise based on experiments done at 24 °C (47). Through imaging flow cytometry, the shape change was confirmed to be highly correlated with the existence of intracellular HbS polymers identified by transmission electron microscopy (TEM) in a recent study (37). Our hypoxia assay is expected to have a higher efficacy for identifying sickled RBCs, because it can incorporate another visual characteristic, cell texture, in addition to changes in cell morphology. The majority of sickled cells (density fractions 1–3) had apparent shape change. Very few sickled cells, especially in density 4, showed little or no apparent shape change but notable changes in cell texture, sharing similar features to the ones at rapid DeOxy rates by O_2 reducing agents (25, 31). The rather low sickled fractions found in Fig. 3 at relatively high %HbS, especially under the short-term DeOxy state, is consistent with the implication that most cells are prevented from sickling in vivo or under physiologically relevant conditions (10).

The kinetics of cell sickling was markedly affected by HU therapy, including delay time of cell sickling ($P < 0.01$ for 5% and 10% of sickled fractions; $P < 0.02$ for saturated sickled fraction) and maximum sickled ratio under the short-term hypoxia state ($P = 0.03$). This analysis highlighted the beneficial effects of HU therapy on DeOxy sickle RBCs. These results are consistent with previous clinical reports of disease amelioration through the stimulation of HbF synthesis (48–51). Additionally, we identified outlier patient samples (marked by arrows in Figs. 3 *A* and *C* and 4*C*) that showed the most abnormal results in our assays, including shortest delay time of cell sickling, highest sickled fraction, and highest capillary obstruction ratio, all suggesting high risk for vasoocclusion. Hematological measurements indicated these two patient samples to be severe SCD, according to a genotype-based disease severity classification (52). Our analysis also indicated that HbF levels do not completely account for the kinetics of cell sickling, including the maximum sickled fraction ($R = -0.4$, $P = 0.05$ for short-term hypoxia state; $R = -0.55$, $P = 0.005$ for long-term hypoxia state) and the delay time of cell sickling ($R = 0.35$, $P = 0.08$ at a low sickled fraction, 5%). These observations are consistent with studies indicating only partial correlation between HbF fraction and painful crises (16, 20, 22). The large variations in delay time of cell sickling in the on-HU group could correlate with additional outcomes from HU therapy besides HbF induction (53, 54). Therefore, our analysis could offer a unique route to developing a supplementary tool at cellular

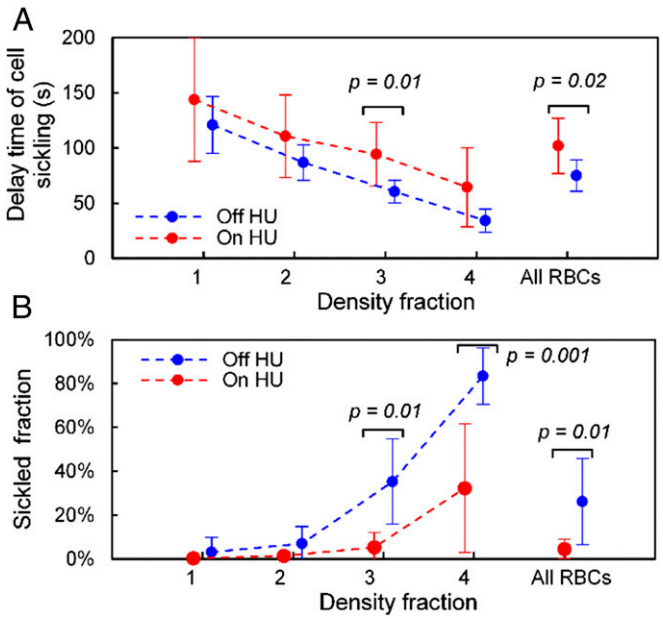

Fig. 5. Role of cell density. (*A*) Delay time of cell sickling and (*B*) sickled fraction under the short-term DeOxy state. Error bars indicate standard deviations.

level, beyond current hematological assays (55), to evaluate the response to HU and other antisickling drugs for individual SCD patients. An example of this is found with Aes-103 (5-hydroxymethylfurfural), which is currently in phase II clinical trials in SCD patients. The sickled fraction after a long-term hypoxia in sickle RBCs incubated with Aes-103 in vitro showed a strong correlation with the drug concentration (*SI Text*, *Antisickling Drug* and Fig. S7). This finding is consistent with a previous study (36).

Further analysis of sickling considered hydration state and Hb types. There was no correlation of effective sickled fraction (sickled fraction*) (*SI Text*, *Effective Sickled Fraction* and Fig. S8) with MCHC-F ($R = -0.17$, $P = 0.22$) but strong correlation with MCHC-S ($R = 0.71$, $P < 0.001$). These observations indicate that clinical hematological information alone cannot be used to evaluate cell sickling events in vitro. Further analysis showed a lack of correlation between the sickled fraction* and MCHC-S/F (by multiplying the MCHC value with the ratio of %HbS to %HbF), suggesting that MCHC-S is a determinant factor in cell sickling in vitro. These results also imply that when investigating the influence of HbF, the average concentration of HbF in a cell population is less important than the HbF content in individual RBCs (53). This interpretation is supported by an ex vivo study showing incomplete resistance of F cells in hypoxia-induced sickling (56).

The mean velocity of individual sickle RBCs is an integrative measure modulated by cell size, shape, intracellular viscosity, and membrane deformability, and could potentially serve as a direct indicator of the ability of cells to transit in capillaries. The opposing effects of elevated cell size (57) and increased membrane deformability (58) due to HU therapy both influence cell traversal through microgates. Individual-cell velocity was strongly correlated with cell volume ($R = -0.89$, $P < 0.001$) instead of other hematological measurements, e.g., %HbS, HCT (hematocrit), and MCHC. Cell shape played an important role in transit, especially for the irreversibly sickled cells in the off-HU cases. Additionally, we found that the velocity of deformable cells under the DeOxy state was lower than for cells under the Oxy state, disregarding the influences of HU therapy and transfusion (Fig. S2). This discrepancy may be caused by the increased intracellular viscosity from HbS polymerization and the influence of the degree of oxygenation on HbA (59). The improved rheological properties of sickle RBCs in vivo could therefore stem from the elevated numbers of F cells and the beneficial effects of HbF in cell sickling (57). Similar trends were found in the relationship between sickled fraction and %HbS (Fig. 3*C*) and between capillary obstruction and %HbS (Fig. 4*C*), suggesting that morphologic sickling is likely a primary factor in occlusion in capillaries and small vessels.

Density-dependent kinetics of cell sickling provides quantitative measures of selective adhesion and selective trapping of sickle RBCs (60) in shear flow conditions (61, 62) and in vivo conditions (63). Our observations demonstrated that the lightest cells (density 1) had the longest delay time of sickling and the lowest sickled fraction. This ensured high probability in maintaining deformability for maximum contact area for adhesion during microcirculation, agreeing well with the adhesive dynamics of single sickle RBCs (64). The densest cells (density 4) exhibited the shortest delay time for cell sickling, the highest sickled fraction, and the longest delay time for cell unsickling, which may contribute to quick stiffening and ready trapping.

We found that the beneficial effects of HU therapy on sickling kinetics were more evident for the relatively dense populations, in terms of the delay time of cell sickling ($P = 0.01$ and $P = 0.06$ for density 3 and density 4, respectively) and the maximum sickled fraction ($P = 0.01$ and $P = 0.001$ for density 3 and density 4, respectively). These factors could serve as candidate biomarkers to evaluate the efficacy of HU therapy and to guide the development of new therapeutics.

Materials and Methods

Sickle RBC Samples. All studies involving human blood were approved by the institutional review board (IRB) of National Institutes of Health (NIH), Massachusetts General Hospital (MGH), and Massachusetts Institute of Technology (MIT). Blood samples from 40 SCD patients, including 26 patients with HU therapy (on-HU), 12 patients without HU therapy (off-HU), and 2 patients off-HU but with transfusion (off-HU/T), were collected in EDTA anticoagulant at NIH and MGH (using written consent forms approved by NIH and MGH IRB, respectively) and shipped to MIT on ice and stored at 4 °C. All of the microfluidics tests were conducted within 3 d of blood drawing. For cell sickling/unsickling tests, we used 25 samples (18 on-HU and 7 off-HU). For the single-cell rheology test, we used 15 samples, including 6 on-HU, 7 off-HU, and 2 off-HU/T. For the study of cell density, we used 20 samples, including 14 on-HU and 6 off-HU. Another 13 samples (8 on-HU and 5 off-HU) were used for HPLC characterization. For Aes-103 testing, blood samples from 3 on-HU and 3 off-HU patients were incubated with Aes-103 at different concentrations (0.5, 1, 2, and 5 mM) for 1 h at 37 °C before the in vitro sickling test.

Sickle RBC fractionation according to cell density was performed by means of a stepwise gradient prepared with OptiPrep solution with density adjusted with Dulbecco's PBS (HyClone DPBS; Thermo Scientific) based on the specific gravity. The fractionation gradient was built up with four layers of 2.5 mL OptiPrep-DPBS medium of densities 1.081, 1.091, 1.100, and 1.111 g/mL, respectively. A 1-mL blood sample was washed twice with PBS at 821 × *g* for 5 min at 21 °C and diluted into 70~80% hematocrit. Then, the RBC pellet was fully suspended by gentle vortexing and layered on top of the gradient. Cell fractionation was achieved by a 30-min centrifugation at 821 × *g* and 21 °C. The four fractionated populations trapped between the interfaces of successive layers of gradient medium and in the bottom of the tube were carefully collected with a 1-mL pipette tip and washed with 5 mL PBS buffer twice to remove gradient residue. The four fractions, density 1–4, have mean densities of 1.086 ± 0.005 g/mL, 1.095 ± 0.005 g/mL, 1.105 ± 0.005 g/mL, and >1.111 g/mL, respectively. Fractionated sickle RBCs were then suspended with RPMI-1640 containing 1% (wt/vol) BSA (Sigma-Aldrich) and stored at 4 °C until shortly before use to avoid metabolic depletion. BSA was used to maintain the cellular livability and prevent cell adhesion to the interior surfaces of microfluidic devices.

Microfluidic Platform. Microfluidic devices were designed and fabricated using polydimethylsiloxane casting protocols and bonded to microscope slides. The masters of PDMS channels were fabricated with silicon wafers using standard photolithography techniques and followed with 2-h surface passivation using fluorinated silane vapor [(tridecafluoro-1,1,2,2-tetrahydrooctyl)-1-trichlorosilane; T2492-KG; United Chemical Technologies]. O_2 concentration in the cell channel was controlled by the gas flow in the gas channel. The transient hypoxia condition was created by switching between two gas mixtures, including a gas mixture of 5% CO_2, 20% O_2 with N_2 balance for an initial oxygenation and reoxygenation and a gas mixture of 5% CO_2, 2% O_2 with N_2 balance for deoxygenation. Two reservoirs (1.5 mm in diameter and 2 mm deep) for cell buffer exchange were fabricated 1.2 mm away from the obstacles and connected to the external hydraulic columns via flexible Tygon microbore tubing (0.020 inch i.d. × 0.060 inch o.d.). Before the rheology test, the microfluidic devices were degassed for at least 15 min before filling with working medium to improve wetting and prevent air bubble trapping.

Experimental Conditions. Experiments were performed on a Zeiss Axiovert 200 inverted microscope using a halogen source (100 W). Microfluidic devices were enclosed in a heating incubator (ibidi heating system) with temperature maintained at 37 °C for both cell sickling and rheology measurements. The temperature state of the cell buffer within the microfluidic channel was calibrated with a thermocouple considering the mass exchange (gas and cell buffer) before the experiment. Images of RBCs were enhanced with a 414/446-nm band-pass filter (Semrock). Local O_2 concentration in the cell channel was characterized offline using Tris(4,7-diphenyl-1,10-phenanthroline) ruthenium (II) dichloride complex [$Ru(dpp)_3Cl_2$; Sigma-Aldrich], the fluorescence of which is strongly reduced by molecular O_2 due to dynamic quenching. Because $Ru(dpp)_3Cl_2$ is water-insoluble, it was dissolved in acetone-RPMI (volume ratio of 1:2) at 0.8 mg/mL and injected into the cell channel. Luminescence was measured at an emission wavelength of 488 nm. Short-term and long-term hypoxia conditions held the durations of the DeOxy state (O_2 concentration <5%) at about 25 and 220 s, respectively. The division of 5% was selected because sickle RBCs start to sickle when O_2 is lower than this point.

HPLC. The relative proportions of HbS, HbF, HbA, and HbA2 of density-separated cell populations were obtained via HPLC performed at Brigham and Women's Hospital.

Statistical Study. All data are expressed as mean ± SD. Statistical analyses were performed with OriginPro 8 (OriginLab). A two-sample *t* test between measurements of samples from on-HU patients and off-HU patients was used to generate the *P* values with equal variance not assumed. Correlation analyses between the biophysical measurements and the hematological values were performed using Pearson's correlation.

ACKNOWLEDGMENTS. The authors thank Dr. John Higgins for providing SCD blood samples and for helpful discussions, and thank Ms. Laurel Medelsohn and Mr. James Nichols at NIH for assistance in procuring sickle cell blood samples. E.D., M.D.-S., and M.D. acknowledge support by the NIH (R01HL094270 and U01HL114476). S.S. acknowledges support from Carnegie Mellon University.

1. Ballas SK, Gupta K, Adams-Graves P (2012) Sickle cell pain: A critical reappraisal. *Blood* 120(18):3647–3656.
2. Castro O, et al.; The Cooperative Study of Sickle Cell Disease (1994) The acute chest syndrome in sickle cell disease: Incidence and risk factors. *Blood* 84(2):643–649.
3. van Beers EJ, van der Giessen A, van Tuijn CFJ, Schnog JJ, Biemond BJ (2006) Systematic evaluation of sickle cell-related organ damage and complications: Implications for sickle cell disease management. *Blood* 108(11):25b.
4. Pegelow CH, et al. (1997) Natural history of blood pressure in sickle cell disease: Risks for stroke and death associated with relative hypertension in sickle cell anemia. *Am J Med* 102(2):171–177.
5. Machado RF, et al. (2011) NT-pro brain natriuretic peptide levels and the risk of death in the cooperative study of sickle cell disease. *Br J Haematol* 154(4):512–520.
6. Embury SH (2004) The not-so-simple process of sickle cell vasoocclusion. *Microcirculation* 11(2):101–113.
7. Frenette PS (2002) Sickle cell vaso-occlusion: Multistep and multicellular paradigm. *Curr Opin Hematol* 9(2):101–106.
8. Barabino GA, Platt MO, Kaul DK (2010) Sickle cell biomechanics. *Annu Rev Biomed Eng* 12:345–367.
9. Eaton WA, Hofrichter J (1987) Hemoglobin S gelation and sickle cell disease. *Blood* 70(5):1245–1266.
10. Mozzarelli A, Hofrichter J, Eaton WA (1987) Delay time of hemoglobin S polymerization prevents most cells from sickling in vivo. *Science* 237(4814):500–506.
11. Eaton WA, Hofrichter J, Ross PD (1976) Editorial: Delay time of gelation: A possible determinant of clinical severity in sickle cell disease. *Blood* 47(4):621–627.
12. Higgins JM, Eddington DT, Bhatia SN, Mahadevan L (2007) Sickle cell vasoocclusion and rescue in a microfluidic device. *Proc Natl Acad Sci USA* 104(51):20496–20500.
13. Kaul DK, Nagel RL, Baez S (1983) Pressure effects on the flow behavior of sickle (HbSS) red cells in isolated (ex-vivo) microvascular system. *Microvasc Res* 26(2):170–181.
14. Platt OS, et al. (1991) Pain in sickle cell disease. Rates and risk factors. *N Engl J Med* 325(1):11–16.
15. Platt OS, et al. (1994) Mortality in sickle cell disease. Life expectancy and risk factors for early death. *N Engl J Med* 330(23):1639–1644.
16. Powars DR, Schroeder WA, Weiss JN, Chan LS, Azen SP (1980) Lack of influence of fetal hemoglobin levels or erythrocyte indices on the severity of sickle cell anemia. *J Clin Invest* 65(3):732–740.
17. Poillon WN, Kim BC, Castro O (1998) Intracellular hemoglobin S polymerization and the clinical severity of sickle cell anemia. *Blood* 91(5):1777–1783.
18. Billett HH, Kim K, Fabry ME, Nagel RL (1986) The percentage of dense red cells does not predict incidence of sickle cell painful crisis. *Blood* 68(1):301–303.
19. Odenheimer DJ, Sarnaik SA, Whitten CF, Rucknagel DL, Sing CF (1987) The relationship between fetal hemoglobin and disease severity in children with sickle cell anemia. *Am J Med Genet* 27(3):525–535.
20. Akinsheye I, et al. (2011) Fetal hemoglobin in sickle cell anemia. *Blood* 118(1):19–27.
21. Lande WM, et al. (1988) The incidence of painful crisis in homozygous sickle cell disease: Correlation with red cell deformability. *Blood* 72(6):2056–2059.
22. Ballas SK, et al. (1988) Rheologic predictors of the severity of the painful sickle cell crisis. *Blood* 72(4):1216–1223.
23. Ballas SK, Smith ED (1992) Red blood cell changes during the evolution of the sickle cell painful crisis. *Blood* 79(8):2154–2163.
24. Wood DK, Soriano A, Mahadevan L, Higgins JM, Bhatia SN (2012) A biophysical indicator of vaso-occlusive risk in sickle cell disease. *Sci Transl Med* 4(123):123ra26.
25. Abbyad P, Tharaux PL, Martin JL, Baroud CN, Alexandrou A (2010) Sickling of red blood cells through rapid oxygen exchange in microfluidic drops. *Lab Chip* 10(19):2505–2512.
26. Tsai M, et al. (2012) In vitro modeling of the microvascular occlusion and thrombosis that occur in hematologic diseases using microfluidic technology. *J Clin Invest* 122(1):408–418.
27. Asakura T, et al. (1994) Partially oxygenated sickled cells: Sickle-shaped red cells found in circulating blood of patients with sickle cell disease. *Proc Natl Acad Sci USA* 91(26):12589–12593.
28. Itoh T, Chien S, Usami S (1992) Deformability measurements on individual sickle cells using a new system with pO_2 and temperature control. *Blood* 79(8):2141–2147.
29. Takashima S, Chang S, Asakura T (1985) Shape change of sickled erythrocytes induced by pulsed rf electrical fields. *Proc Natl Acad Sci USA* 82(20):6860–6864.
30. Kueh HY, Brieher WM, Mitchison TJ (2008) Dynamic stabilization of actin filaments. *Proc Natl Acad Sci USA* 105(43):16531–16536.
31. Christoph GW, Hofrichter J, Eaton WA (2005) Understanding the shape of sickled red cells. *Biophys J* 88(2):1371–1376.
32. Coletta M, Hofrichter J, Ferrone FA, Eaton WA (1982) Kinetics of sickle haemoglobin polymerization in single red cells. *Nature* 300(5888):194–197.
33. Kniazeva T, Hsiao JC, Charest JL, Borenstein JT (2011) A microfluidic respiratory assist device with high gas permeance for artificial lung applications. *Biomed Microdevices* 13(2):315–323.
34. Kaul DK, Xue H (1991) Rate of deoxygenation and rheologic behavior of blood in sickle cell anemia. *Blood* 77(6):1353–1361.
35. Krause WJ (2005) *Krause's Essential Human Histology for Medical Students* (Universal, Boca Raton, FL), 3rd Ed.
36. Abdulmalik O, et al. (2005) 5-Hydroxymethyl-2-furfural modifies intracellular sickle haemoglobin and inhibits sickling of red blood cells. *Br J Haematol* 128(4):552–561.
37. van Beers EJ, et al. (2014) Imaging flow cytometry for automated detection of hypoxia-induced erythrocyte shape change in sickle cell disease. *Am J Hematol* 89(6):598–603.
38. Itoh T, Chien S, Usami S (1995) Effects of hemoglobin concentration on deformability of individual sickle cells after deoxygenation. *Blood* 85(8):2245–2253.
39. Kaul DK, Liu XD (1999) Rate of deoxygenation modulates rheologic behavior of sickle red blood cells at a given mean corpuscular hemoglobin concentration. *Clin Hemorheol Microcirc* 21(2):125–135.
40. Corbett JD, Mickols WE, Maestre MF (1995) Effect of hemoglobin concentration on nucleation and polymer formation in sickle red blood cells. *J Biol Chem* 270(6):2708–2715.
41. Schwartz RS, Musto S, Fabry ME, Nagel RL (1998) Two distinct pathways mediate the formation of intermediate density cells and hyperdense cells from normal density sickle red blood cells. *Blood* 92(12):4844–4855.
42. Brugnara C (1995) Erythrocyte dehydration in pathophysiology and treatment of sickle cell disease. *Curr Opin Hematol* 2(2):132–138.
43. Makhijani VB, Cokelet GR (1994) In vivo polymerization of sickle-cell hemoglobin: A theoretical study. *Blood Cells* 20(1):169–183, discussion 184–190.
44. Vekilov PG (2007) Sickle-cell haemoglobin polymerization: Is it the primary pathogenic event of sickle-cell anaemia? *Br J Haematol* 139(2):173–184.
45. Basu S, et al. (2011) F-cell levels are altered with erythrocyte density in sickle cell disease. *Blood Cells Mol Dis* 47(2):117–119.
46. Yasin Z, et al. (2003) Phosphatidylserine externalization in sickle red blood cells: Associations with cell age, density, and hemoglobin F. *Blood* 102(1):365–370.
47. Hiruma H, et al. (1995) Sickle cell rheology is determined by polymer fraction—not cell morphology. *Am J Hematol* 48(1):19–28.
48. Charache S, et al.; Investigators of the Multicenter Study of Hydroxyurea in Sickle Cell Anemia (1995) Effect of hydroxyurea on the frequency of painful crises in sickle cell anemia. *N Engl J Med* 332(20):1317–1322.
49. Davies SC, Gilmore A (2003) The role of hydroxyurea in the management of sickle cell disease. *Blood Rev* 17(2):99–109.
50. Rodgers GP, Dover GJ, Noguchi CT, Schechter AN, Nienhuis AW (1990) Hematologic responses of patients with sickle cell disease to treatment with hydroxyurea. *N Engl J Med* 322(15):1037–1045.
51. Charache S, et al. (1992) Hydroxyurea: Effects on hemoglobin F production in patients with sickle cell anemia. *Blood* 79(10):2555–2565.
52. Rees DC, Williams TN, Gladwin MT (2010) Sickle-cell disease. *Lancet* 376(9757):2018–2031.
53. Steinberg MH, Chui DHK, Dover GJ, Sebastiani P, Alsultan A (2014) Fetal hemoglobin in sickle cell anemia: A glass half full? *Blood* 123(4):481–485.
54. Segel GB, Simon W, Lichtman MA (2011) Should we still be focused on red cell hemoglobin F as the principal explanation for the salutary effect of hydroxyurea in sickle cell disease? *Pediatr Blood Cancer* 57(1):8–9.
55. Steinberg MH, et al.; Multicenter Study of Hydroxyurea (1997) Fetal hemoglobin in sickle cell anemia: Determinants of response to hydroxyurea. *Blood* 89(3):1078–1088.
56. Fertrin KY, et al. (2014) Imaging flow cytometry documents incomplete resistance of human sickle F-cells to ex vivo hypoxia-induced sickling. *Blood* 124(4):658–660.
57. Orringer EP, et al. (1991) Effects of hydroxyurea on hemoglobin F and water content in the red blood cells of dogs and of patients with sickle cell anemia. *Blood* 78(1):212–216.
58. Ballas SK, Dover GJ, Charache S (1989) Effect of hydroxyurea on the rheological properties of sickle erythrocytes in vivo. *Am J Hematol* 32(2):104–111.
59. Uyuklu M, Meiselman HJ, Baskurt OK (2009) Effect of hemoglobin oxygenation level on red blood cell deformability and aggregation parameters. *Clin Hemorheol Microcirc* 41(3):179–188.
60. Kaul DK, Finnegan E, Barabino GA (2009) Sickle red cell-endothelium interactions. *Microcirculation* 16(1):97–111.
61. Barabino GA, McIntire LV, Eskin SG, Sears DA, Udden M (1987) Endothelial cell interactions with sickle cell, sickle trait, mechanically injured, and normal erythrocytes under controlled flow. *Blood* 70(1):152–157.
62. Kaul DK, Fabry ME, Nagel RL (1989) Microvascular sites and characteristics of sickle cell adhesion to vascular endothelium in shear flow conditions: Pathophysiological implications. *Proc Natl Acad Sci USA* 86(9):3356–3360.
63. Kaul DK, Fabry ME (2004) In vivo studies of sickle red blood cells. *Microcirculation* 11(2):153–165.
64. Lei H, Karniadakis GE (2013) Probing vasoocclusion phenomena in sickle cell anemia via mesoscopic simulations. *Proc Natl Acad Sci USA* 110(28):11326–11330.